frontiers | Frontiers in Energy Research

TYPE Original Research
PUBLISHED 15 September 2022
DOI 10.3389/fenrg.2022.1008042

OPEN ACCESS

EDITED BY
Mohamed A. Mohamed,
Minia University, Egypt

REVIEWED BY
Hong Tan,
China Three Gorges University, China
Hassan Farh,
Hong Kong Polytechnic University,
Hong Kong SAR, China

*CORRESPONDENCE
Shiduo Jia,
jiashiduo@stu.xjtu.edu.cn
Xiaoning Kang,
kangxn@mail.xjtu.edu.cn

SPECIALTY SECTION
This article was submitted to Smart Grids,
a section of the journal
Frontiers in Energy Research

RECEIVED 31 July 2022
ACCEPTED 24 August 2022
PUBLISHED 15 September 2022

CITATION
Jia S, Kang X, Cui J, Tian B, Zhang J and Xiao S (2022), Multi-layer coordinated optimization of integrated energy system with electric vehicles based on feedback correction.
Front. Energy Res. 10:1008042.
doi: 10.3389/fenrg.2022.1008042

Multi-layer coordinated optimization of integrated energy system with electric vehicles based on feedback correction

Shiduo Jia*, Xiaoning Kang*, Jinxu Cui, Bowen Tian, Jiawei Zhang and Shuwen Xiao

Shaanxi Key Laboratory of Smart Grid, Xi'an Jiaotong University, Xi'an, China

The integrated energy system with electric vehicles can realize multi-energy coordination and complementarity, and effectively promote the realization of low-carbon environmental protection goals. However, the temporary change of vehicle travel plan will have an adverse impact on the system. Therefore, a multi-layer coordinated optimization strategy of electric-thermal-hydrogen integrated energy system including vehicle to grid (V2G) load feedback correction is proposed. The strategy is based on the coordination of three-level optimization. The electric vehicle charging and discharging management layer comprehensively considers the variance of load curve and the dissatisfaction of vehicle owners, and the charging and discharging plan is obtained through multi-objective improved sparrow search algorithm, which is transferred to the model predictive control rolling optimization layer. In the rolling optimization process, according to the actual situation, selectively enter the V2G load feedback correction layer to update V2G load, so as to eliminate the impact of temporary changes in electric vehicle travel plans. Simulation results show that the total operating cost with feedback correction is 4.19% lower than that without feedback correction and tracking situation of tie-line planned value is improved, which verifies the proposed strategy.

KEYWORDS

electric vehicle, V2G, electric-thermal-hydrogen integrated energy system, multilayer coordinated optimization, sparrow search algorithm

1 Introduction

In order to solve global environmental problems, it is necessary to build a clean and low-carbon new energy system. The integrated energy system effectively improves the energy utilization efficiency and promotes the consumption of renewable energy through the multi energy coupling mechanism, thereby reducing carbon emissions (Ding et al., 2018; Yang et al., 2018; Cheng et al., 2019). The interaction between electric vehicle (EV) and integrated energy system can further tap flexible resources and promote the carbon

reduction operation of the system (Zhou et al., 2021; Li et al., 2022). EVs can be connected to the power grid as mobile loads, and they have the characteristics of energy storage (Hu et al., 2015; Cheng et al., 2021). In order to take advantages of its characteristics, the vehicle to grid (V2G) mode has been proposed in recent years (Wang et al., 2015). Peak shaving and valley filling of load curve can be achieved by managing the charge and discharge of electric vehicles. However, the temporary change of EV travel plan will have an adverse impact on the economic and stable operation of the system.

In practice, EV travel plans are uncertain, and the photovoltaic power, wind power and predicted load power of electric-thermal-hydrogen integrated energy system (ETH-IES) also have randomness and volatility. Considering the characteristics that the prediction accuracy improves with the reduction of time scale, multi-time scale strategy is often used in energy management of integrated energy system (Yin et al., 2020; Tang et al., 2021; Wang et al., 2021). On the larger time range, the unit combination and the base value of operation plan is formulated based on the forecast data. On the smaller time range, the deviation left by the superior is corrected based on the real-time data. On this basis, according to the relationship between different nodes in the optimization process, the energy management is divided into static scheduling and dynamic scheduling. Static scheduling is the optimization of single section, and there will be a large power deviation in actual operation (Qi et al., 2022). Static optimization can be solved by nonlinear programming (Lv et al., 2016) and chance constrained programming (Li et al.,. 2019). Dynamic optimal scheduling considers the connections between different time nodes, and has better robustness (Huang et al., 2014). Generally, model predictive control (MPC) is used for dynamic optimal scheduling. Based on the idea of rolling optimization and feedback correction, it can well solve the optimal control problems with many uncertain factors (Xiao et al., 2016). In addition, unlike the day ahead optimal scheduling, MPC has higher accuracy, because it can continuously obtain real-time short-term power prediction information. The results of each rolling optimization correct the real-time state of the system, which can eliminate the influence of uncertainties on the optimal scheduling scheme to a greater extent (Zhang et al., 2017). At present, many researches apply rolling optimization to the scheduling of integrated energy system, but less to the joint optimal scheduling of system and electric vehicles.

In recent years, more and more studies on the optimal scheduling of integrated energy system with EVs have been published. Reference (Wang et al., 2016) establishes a multi-objective optimization model with optimal generation cost and environmental benefit of microgrid with EVs. Reference (Chen et al., 2020) proposes a fuzzy control algorithm to formulate EV charging plan. The proposed strategy has good real-time performance, but ignores the V2G machanism. Reference (Hou et al., 2019) optimizes the microgrid and EVs according to three levels, which can maximize the benefits. In (Jozi et al., 2022), EV charging and discharging plans are optimally scheduled to maximize parking profits and improve system reliability; Reference (Hu et al., 2019) proposes a real-time scheduling method to smooth photovoltaic power fluctuations through the flexibility of charging and discharging of clustered EVs; Reference (Zhao et al., 2016) motivates EV owners to participate in the dispatching of microgrid by adjusting the electricity price. The above references only formulate energy management strategies from the perspective of micro network operators, ignoring the interests of EV owners. Reference (Cheng et al., 2022) establishes a stochastic optimal scheduling model considering the forecast error of wind power output; Reference (Jia and Kang, 2022) quantifies the uncertainty of wind and photovoltaic output with the conditional value at risk of relative disturbance. Although the above literatures consider the uncertainty of distributed generators and load forecasting power, they ignore the uncertainty of EV travel plans. Reference (Wang et al., 2022) establishes a multi-stage optimal energy management system for participating in the deregulated electricity market. However, reference (Wang et al., 2022) does not consider electric vehicles. In (Alireza et al., 2021), a two-stage operation is presented according to day-ahead and 5 min real time energy markets. However, it uses non-layered architecture to optimize EV charging and discharging and does not consider EV owners' feeling. Reference (Jia et al., 2022) proposes a hierarchical stochastic optimal scheduling model and it uses stochastic programming to deal with uncertainty. In real-time operation, when the number of unplanned EVs suddenly increases, the strategy cannot make corresponding corrections. Furthermore, reference (Jia et al., 2022) adopts static optimal strategy and there will be a large power deviation in actual operation.

For the adverse impact of temporary change in EV travel plan on system operation, this paper establishes a multi-layer coordinated optimization strategy of electric-thermal-hydrogen integrated energy system including the feedback correction of V2G load. On the basis of building the system model, EVs and ETH-IES are optimized hierarchically and solved by multi-objective improved sparrow search algorithm. Furthermore, in order to reduce the impact of temporary changes in EV travel plans, V2G load feedback correction layer is introduced. In the process of rolling optimization of the system, EV unplanned behaviors are identified and the charging and discharging plan is adjusted in time. Finally, taking an electric-thermal-hydrogen integrated energy industrial park as an example, the effectiveness of the proposed strategy is verified. The contributions of this paper are to:

1) Constructing multi-objective EV charging and discharging management model and two-stage MPC rolling optimization model to achieve accurate and economic formulation.

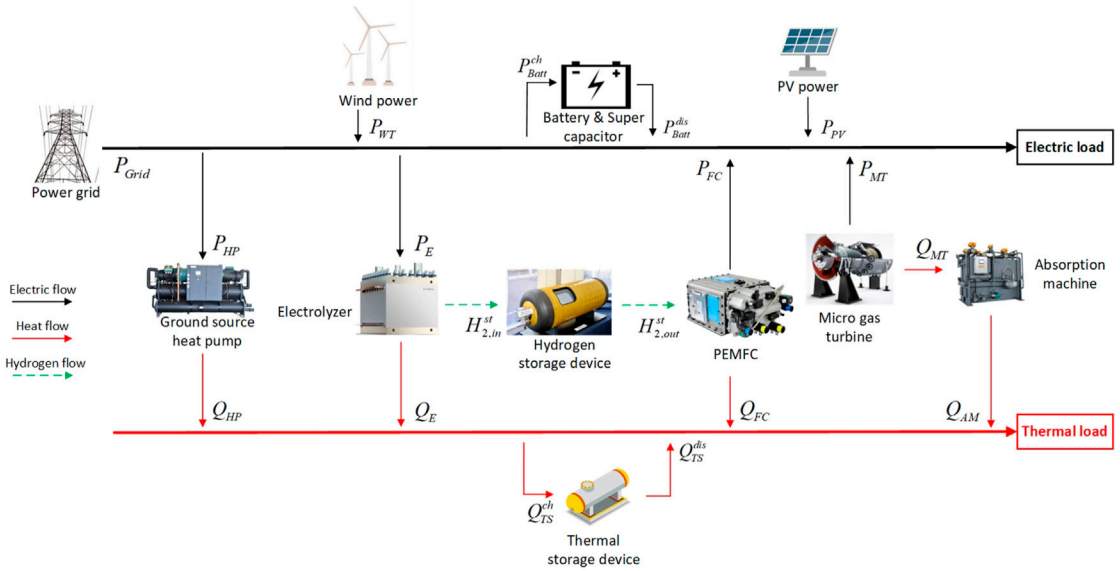

FIGURE 1
Electric-Thermal-Hydrogen integrated energy system architecture.

2) Presenting a multi-layer coordinated optimal scheduling model to improve the economy and stability of system operation, and improves the tracking situation of tie-line planned value.
3) Using the coupled Monte Carlo simulation and multi-objective improved sparrow search algorithm to solve the multi-scenario multi-objective optimal scheduling model.
4) Conducting simulation studies to verify the effectiveness of V2G load feedback correction layer and discussing the effect of the unplanned EVs' proportion on scheduling results.

The rest of the study proceeds as follows: Section 2 introduces the architecture of ETH-IES; Section 3 presents multi-layer coordinated optimization framework based on feedback correction; Section 4 introduces the multi-layer coordinated optimization model in detail. In Section 5, the multi-objective improved sparrow search algorithm is proposed. Section 6 verifies the effectiveness of the V2G load feedback correction layer and discusses the effects of the unplanned EVs' proportion on scheduling results. Finally, Section 7 draws the main conclusions.

2 Architecture of electric-thermal-hydrogen integrated energy system

As shown in Figure 1, the main equipment of ETH-IES includes hydrogen storage device, electrolyzer, proton exchange membrane fuel cell (PEMFC), thermal storage device, super capacitor, battery, wind turbine, photovoltaic, ground source heat pump, absorption machine and micro gas turbine. Among them, micro gas turbine and ground source heat pump unit belong to electrothermal coupling equipment, while electrolyzer and PEMFC belong to electric-thermal-hydrogen coupling equipment. Their introduction can not only realize multi-energy coordination and complementarity, but also improve the system operation flexibility and economy.

2.1 Conventional unit model

In the proposed electric-thermal-hydrogen integrated energy system architecture, the mathematical models of micro gas turbine, ground source heat pump and absorption refrigeration unit can be referred to reference (Li et al., 2021), and the models of wind turbine, photovoltaic and energy storage device can be found in reference (Jia et al., 2022). Due to limited space, this paper only introduces the models of electrolyzer, hydrogen storage device and proton exchange membrane fuel cell in detail.

2.2 Proton exchange membrane fuel cell model

The PEMFC output voltage is mainly influenced by the concentration polarization, the ohmic polarization and the active polarization, and it can be considered as the difference between the Nernst voltage and the loss voltage caused by them (Colleen, 2008). Activation loss can be expressed by Tafel formula:

$$\Delta v_{\text{act}} = a + b \ln i \tag{1}$$

where, $a = -\frac{RT}{nF} ln(i_0); b = -\frac{RT}{nF^{\circ}}$

The loss voltage caused by the active polarization could be calculated as:

$$v_{\text{act}} = \frac{RT}{nF\alpha} ln\left(\frac{i}{i_0}\right)_{\text{anode}} + \frac{RT}{nF\alpha} ln\left(\frac{i}{i_0}\right)_{\text{cath}} \tag{2}$$

The loss voltage caused by the ohmic polarization could be calculated as:

$$v_{\text{ohmic}} = -ir \tag{3}$$

The loss voltage caused by the concentration polarization could be calculated as:

$$v_{\text{conc}} = \alpha_1 i_K ln\left(1 - \frac{i}{i_L}\right) \tag{4}$$

To calculate the Nernst voltage, some pressure values of oxygen, water and hydrogen are needed. Refer to (Colleen, 2008), it can be expressed as:

$$E_{\text{Nernst}} = -\frac{G_{\text{f,liq}}}{2F} + \frac{RT_{\text{K}}}{2F} ln\left(\frac{P_{\text{H}_2\text{O}}}{P_{\text{H}_2} P_{\text{O}_2}^{\frac{1}{2}}}\right) \tag{5}$$

To sum up, the actual voltage can be expressed as:

$$V = E_{\text{Nernst}} + v_{\text{act}} + v_{\text{ohmic}} + v_{\text{conc}} \tag{6}$$

2.3 Electrolyzer model

The electrolyzer consumes electric energy to produce heat and hydrogen energy. The relationship between electricity consumption and hydrogen production is approximately linear, which can be expressed as follows:

$$P_t^{EL} = \lambda_{H_2} H_2^{EL,t} \tag{7}$$

2.4 Hydrogen storage device model

The hydrogen stored in the hydrogen storage device at the current moment is related to the storage capacity, outgassing volume and storage volume at the previous moment. Therefore, the hydrogen stored in the device can be expressed as:

$$H_2^{st,t} = H_2^{st,t-1} + H_{2,in}^{st,t-1} - H_{2,out}^{st,t-1} \tag{8}$$

$$P_{sto,t}^{H_2} = \frac{H_2^{st,t} R_c K}{V_{sto} - \text{H}_2^{st,t} b} - \frac{\left(\text{H}_2^{st,t}\right)^2 a}{V_{sto}^2} \tag{9}$$

$$Sohc_t = \frac{P_{sto,t}^{\text{H}_2}}{P_{sto,rated}^{\text{H}_2}} \tag{10}$$

3 Multi-layer coordinated optimization framework for integrated energy system with electric vehicles based on feedback correction

As shown in Figure 2, the multi-layer coordinated optimization framework of ETH-IES proposed in this paper contains three layers altogether: EV charging and discharging management layer, MPC rolling optimization layer and V2G load feedback correction layer. First, the EV charging and discharging management layer simulates EV travel scenarios through Monte Carlo according to owners' historical habit data, optimizes the charging and discharging of EVs in each scenario, and transmits the results to the MPC rolling optimization layer. Secondly, the MPC rolling optimization layer is divided into two stages. In the first stage, economic scheduling is carried out with 24 h as the time window and 1 h as the time step, and the results are passed into the second stage as the reference value. The second stage takes 1 h as the time window and 5 mins as the time step to coordinate the output of each distributed generator according to the received real-time prediction data, so that the tie-line power can track the superior planned value. Finally, during the operation of MPC rolling optimization layer, the number of EVs with temporary change in their travel plan is identified in real time. If the proportion is greater than the threshold, the V2G load feedback correction layer is carried out and the EV charging and discharging plan is re-established. The revised V2G equivalent load is fed back to the MPC rolling optimization layer and the operation continues from the breakpoint. The specific solution flow chart is shown in Figure 3.

4 Multi-layer coordinated optimization model of integrated energy system with electric vehicles

4.1 Electric vehicle charging and discharging management layer

By managing the charging and discharging of electric vehicles, peak shaving and valley filling of the load curve can be achieved. However, the large degradation of EVs battery will greatly increase the dissatisfaction of EV owners. Thus, the degradation cost should be considered in the proposed optimization model.

4.1.1 Electric vehicle degradation cost model

High degradation cost will greatly increase the EV owners dissatisfaction, which embodies in the reduction of cycle number

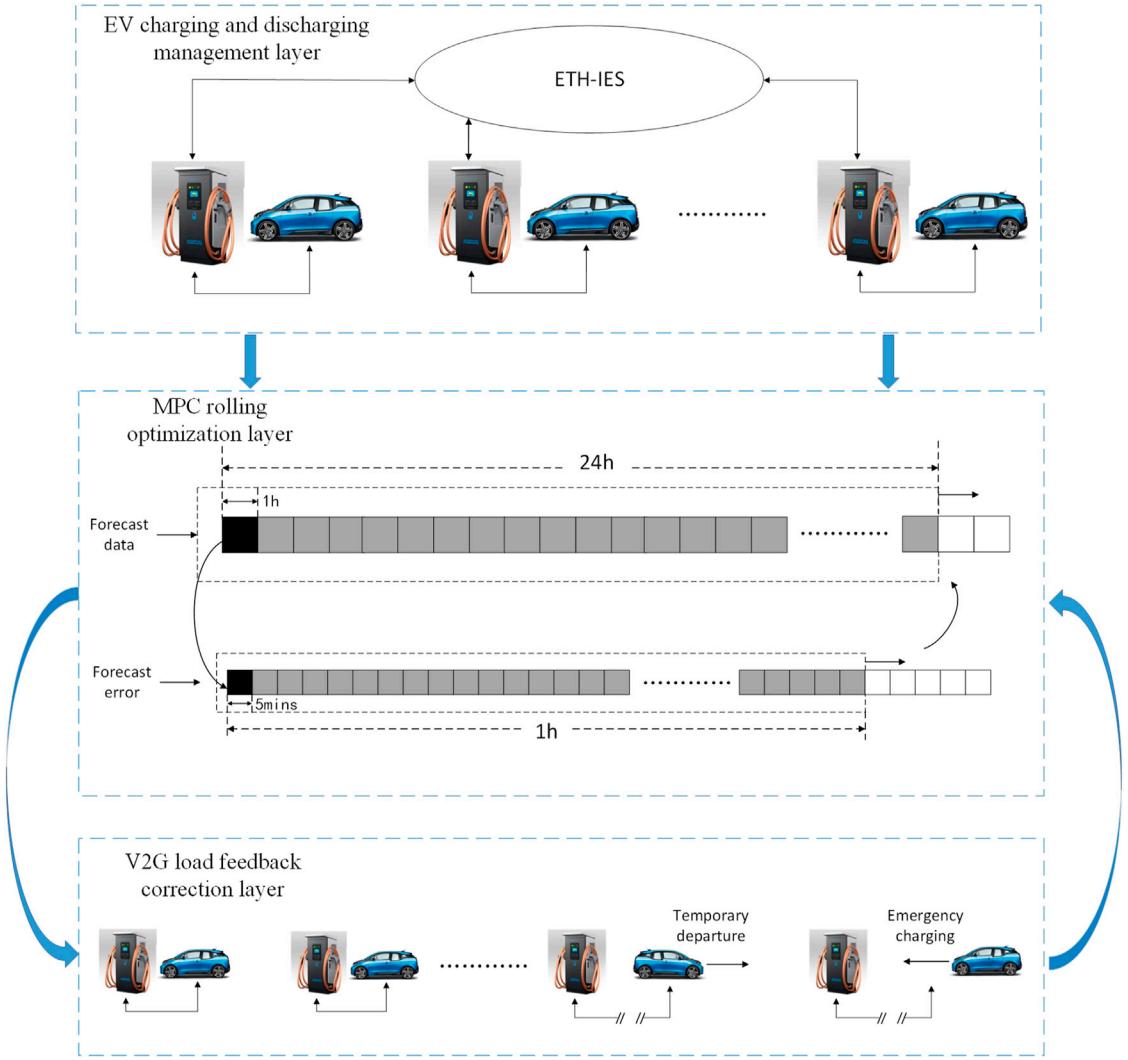

FIGURE 2
ETH-IES multi-layer coordinated optimization framework.

and the actual full capacity (Smith et al., 2012). The times of frequent charging and discharging, charging and discharging rate and other factors will influence the EV degradation cost (Vetter et al., 2005).

After the calculation of discharge of depth (DOD), the degradation cost could be calculated as follows (Ju et al., 2018):

$$C_{Bde}(t, DOD(\Delta t)) = \frac{C_{re} P_B(t) \Delta t}{2L_B(DOD(\Delta t)) E_{BA}(t) DOD(\Delta t) \eta_{Bc} \eta_{Bd}} \tag{11}$$

The cost of battery degradation within each time interval can only be determined after the end of a charging or discharging event. According to (Ju et al., 2018), the expression of the operating cost considering the degradation effect of the battery is shown in Eq. 12.

$$C_B(t) = C_{Bde}\left(t, \frac{E_a(t)}{E_{BA}(t)}\right) - (1 - g(t)) C_{Bde}\left(t, \frac{E_a(t-1)}{E_{BA}(t-1)}\right) \tag{12}$$

4.1.2 Electric vehicle charging and discharging optimization model

The dispersion of time and space and randomness of charging behavior of EVs may greatly increase the peak-to-valley effect of load curve, and the reduction of EV service life will greatly increase the dissatisfaction of owners. On the basis of this, this paper establishes a multi-objective

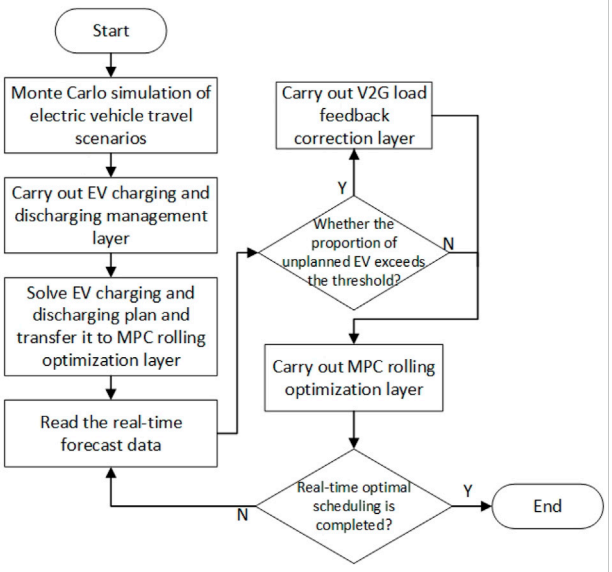

FIGURE 3
ETH-IES multi-layer coordinated optimization flow chat.

optimization model aiming at minimizing the variance of the load curve and minimizing the degradation cost of EVs. Furthermore, the fuzzy membership function (Xu et al., 2015) is used to select the compromise solution from Pareto front as the final solution

1) Objective function 1:

$$minF_1^{EV} = \sum_{t=1}^{T} \frac{1}{T}(P_{load}(t) - Mean(P_{load}))^2 \tag{13}$$

The first objective function is from the system operators' point of view, which aims to decrease the variance of the load curve.

2) Objective function 2:

$$minF_2^{EV} = \frac{\sum_{n=1}^{N_{EV}} \sum_{t=1}^{T} C_B^n(t) - C_B{}^{\min}}{C_B{}^{\max} - C_B{}^{\min}} \tag{14}$$

The second objective function is from the EV owners' point of view. It is a linear function of degradation cost, with a range of 0–1.

3) Constraints:

$$SOC_{\min}^{EV} \le SOC_n^{EV}(t) \le SOC_{\max}^{EV} \tag{15}$$

$$-P_{cha}^{\max} \le P_n^{EV}(t) \le P_{dis}^{\max} \tag{16}$$

$$0 \le I_n^{cha}(t) + I_n^{dis}(t) \le 1 \tag{17}$$

The constraints mainly contain the charging and discharging power limitation and EVs' SOC limitation.

4.2 Model predictive control rolling optimization layer

With the shortening of time step, the accuracy of prediction data is improved. By adjusting the output of distributed power supply, the scheduling economy can be improved and the tie-line power can better track the superior planned value. In addition, the battery is scheduled as a distributed generator, while supercapacitors can stabilize unbalanced power and respond quickly. Therefore, the rolling optimization can be divided into two stages. The short-term optimization stage can improve the operation economy of the system, and the ultra-short-term optimization stage can ensure the safe and stable operation of the system (Ju et al., 2018).

4.2.1 The first stage rolling optimization model

In the first stage, considering the maximum economic benefit, an economic optimization model is established. Since the capacity of the supercapacitor is relatively small compared with other units and its response speed is fast, it is only used to suppress the power prediction error in the second stage.

4.2.1.1 Objective function:

$$minF_1 = F_{utility} + F_{om} + F_{mt} + F_e \tag{18}$$

$$F_{utility} = \sum_{t=1}^{N_t} \left[C_{buy}(t) \cdot P_{Grid\_buy}(t) \cdot \Delta t + C_{sell}(t) \cdot P_{Grid\_sell}(t) \cdot \Delta t\right] \tag{19}$$

$$F_{om} = \sum_{i=1}^{N_i} \sum_{t=1}^{N_t} [|P_i(t)| \cdot K_{om.i} \cdot \Delta t] \tag{20}$$

$$F_{mt} = \sum_{t=1}^{N_t} \left[C_{mt} \cdot f_{mt} \cdot P_{mt}(t) \cdot \Delta t + max\{0, S(t) - S(t-1)\} \cdot C_{mts}\right] \tag{21}$$

$$F_e = \sum_{t=1}^{N_t} \left[CeSO_2 \cdot E_{SO_2}(t) + CeCO_2 \cdot E_{CO_2}(t) + CeNO_x \cdot E_{NO_x}(t)\right] \tag{22}$$

Equations 19–22 respectively represent the switching power cost with the main network, the maintenance cost of distributed power supply, the operation cost of micro gas turbine and the pollution gas treatment cost.

4.2.1.2 Constraints:

1) Constraints on electrothermal power balance:

$$P_{Batt}(t) + P_{MT}(t) + P_{PV}(t) + P_{WT}(t) + P_{Grid}(t) + P_{FC}(t) = P_E(t) + P_{Load}(t) \tag{23}$$

$$Q_{AM}(t) + Q_{HP}(t) + Q_{CS}(t) + Q_{FC}(t) + Q_E(t) = Q_{load}(t) \tag{24}$$

2) Constraints on distributed generator output power:

$$P_{DG.i.\min} \le P_{DG.i} \le P_{DG.i.\max} \tag{25}$$

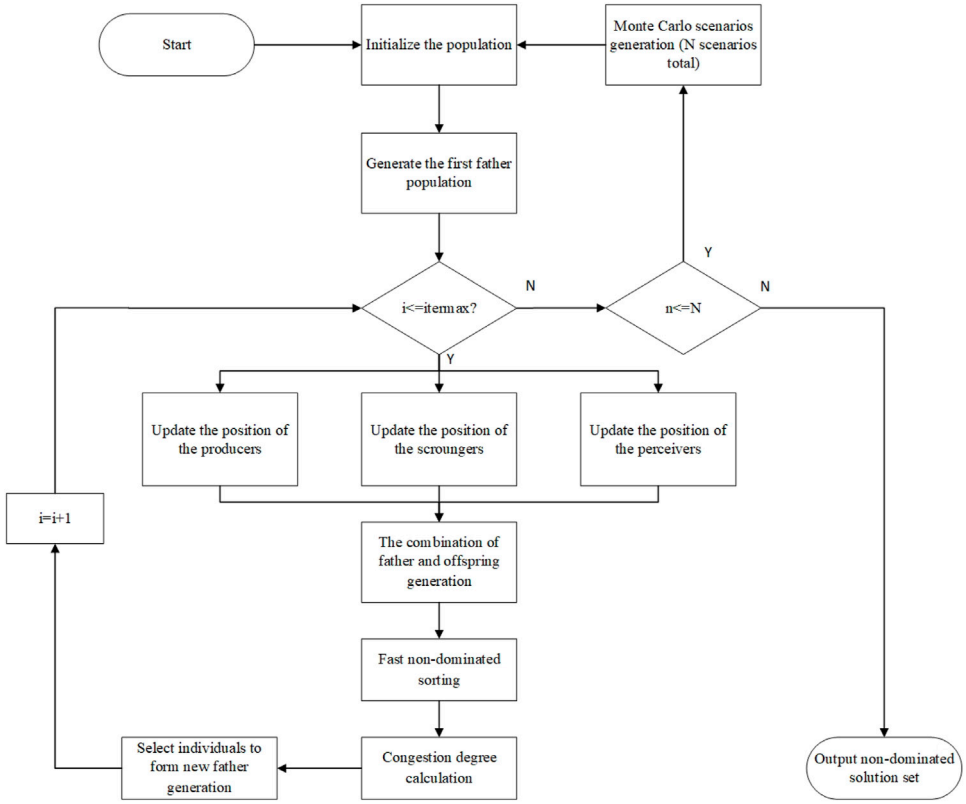

FIGURE 4
Monte Carlo-MISSA algorithm flow chat.

3) Constraints on micro gas turbine ramp rate:

$$\begin{cases} P_{MT}(t) - P_{MT}(t-1) \le R_{up} \cdot \Delta t \\ P_{MT}(t-1) - P_{MT}(t) \le R_{down} \cdot \Delta t \end{cases} \tag{26}$$

4) Constraints on tie-line power:

$$|P_{Grid}(t)| \le P_{Grid.\max} \tag{27}$$

5) Mutual exclusion constraints of electricity purchase and sale signs:

$$U_{Buy}(t) + U_{Sell}(t) \le 1 \tag{28}$$

6) Constraints on micro gas turbine start and stop time:

$$\begin{cases} \sum_{k=1}^{T_{mup}} U_{t-k+1} \ge T_{mup} \\ \sum_{k=1}^{T_{mdown}} (1 - U_{t-k+1}) \ge T_{mdown} \end{cases} \tag{29}$$

7) Battery operation constraints:

$$SOC_{\min} \le SOC(t) \le SOC_{\max} \tag{30}$$

$$-P_{ch.\max} \le P_{Batt}(t) \le P_{dis.\max} \tag{31}$$

$$|SOC(N_t) - SOC(1)| \le \varepsilon \tag{32}$$

$$U_{Batt.ch}(t) + U_{Batt.dis}(t) \le 1 \tag{33}$$

8) Thermal storage device constraints:

$$\lambda_{\min} S_{ES} \le S_{ES}(t) \le \lambda_{\max} S_{ES} \tag{34}$$

$$-Q_{ch.\max} < Q_{CS}(t) < Q_{dis.\max} \tag{35}$$

9) Operation constraints of electrolyzer:

$$P^{EL}_{\min} \le P^{EL}_{t} \le P^{EL}_{\max} \tag{36}$$

$$\Delta P^{EL}_{\min} \le P^{EL}_{t} - P^{EL}_{t-1} \le \Delta P^{EL}_{\max} \tag{37}$$

10) Hydrogen storage device operation constraints:

$$0 \le H^{st,t}_{2,in} \le Y^{H_2}_{st,t} \cdot H^{st,\max}_{2,in} \tag{38}$$

$$0 \le H^{st,t}_{2,out} \le \left(1 - Y^{H_2}_{st,t}\right) \cdot H^{st,\max}_{2,out} \tag{39}$$

$$0 \le H^{st,t}_{2} \le H^{st,rated}_{2} \tag{40}$$

TABLE 1 Random parameters of various EV loads.

Random parameter	Average	Variance
SOC when category ② EVs leave	0.2	0.1
Initial SOC of category ③ EVs	0.3	0.05
Expected SOC of category ③ EVs	0.8	0.05
Departure time of category ② EVs	7:00	30 mins
Return time of category ② EVs	18:00	30 mins
Quantity of category ④ EVs	4	9

TABLE 2 Other related parameters of EV.

Parameter	Value	Parameter	Value
$E_{B.rated}$/kWh	30	$SOC_{\min}/SOC_{\max}$	0.2/0.9
C_{re}/RMB	15 000	$P_{\max}^{\text{char}}/P_{\max}^{\text{dis}}$/kW	7/−7
η_{Bc}	0.9	η_{Bd}	0.9

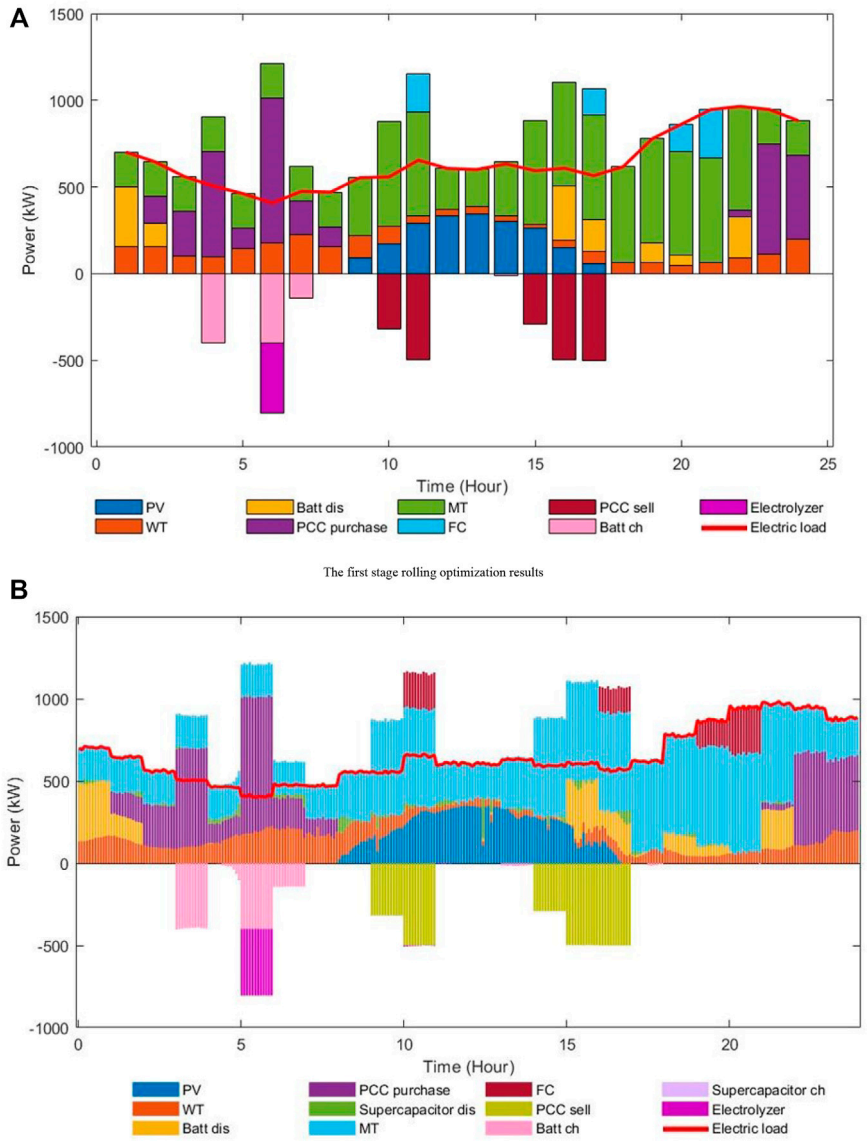

FIGURE 5
Winter electric optimization results of MPC rolling optimization layer. **(A)** The first stage rolling optimization results. **(B)** The second stage rolling optimization results.

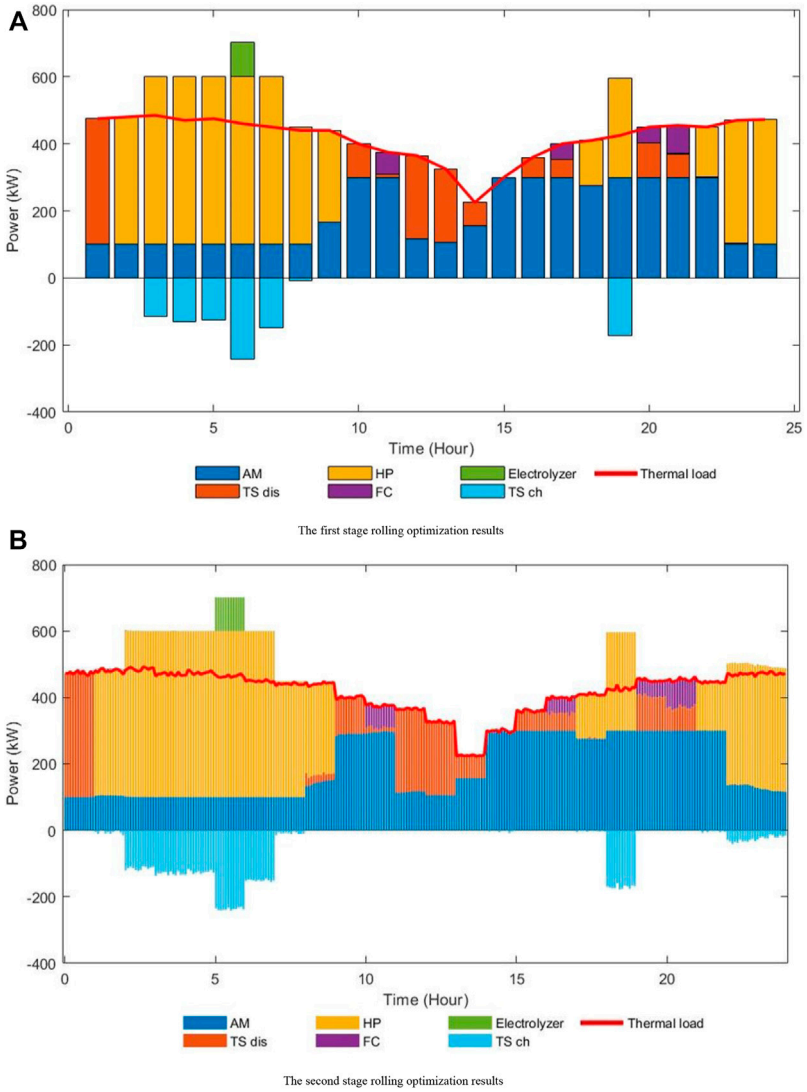

FIGURE 6
Winter thermal optimization results of MPC rolling optimization layer. **(A)** The first stage rolling optimization results. **(B)** The second stage rolling optimization results.

4.2.2 The second stage rolling optimization model

The optimization goal of the second stage is to balance the influence of power prediction error on the basis of the output of each unit obtained in the first stage. The constraint conditions are the same as the first stage, and the objective function is as follows:

$$minF_2 = F_{utility}^{snd} + \sum_{i=1}^{N^{snd}} F_i^{snd} + F_{SC}^{snd} \tag{41}$$

$$F_{utility}^{snd} = \sum_{t=1}^{N_t} \sigma_{utility}^{snd} \left(P_{utility}^{snd}(t) - P_{utility}^{fst}(t) \right)^2 \tag{42}$$

$$F_i^{snd} = \sum_{t=1}^{N_t} \sigma_i^{snd} \left(P_i^{snd}(t) - P_i^{fst}(t) \right)^2 \tag{43}$$

$$F_{SC}^{snd} = \sum_{t=1}^{N_t} K_{om.SC} \cdot P_{SC}^{snd}(t) \tag{44}$$

where $\sigma_{utility}^{snd}$ and σ_i^{snd} are the cost weight coefficient of optimal scheduling in the second stage; $K_{om.SC}$ is the operation and maintenance cost coefficient of supercapacitor; N^{snd} is the number of distributed power supply participating in adjustment in the second stage. Equations 42–44 respectively represent the adjustment cost of tie-line power, the adjustment cost of distributed generators, and the operation and maintenance cost of supercapacitor.

4.3 Vehicle to grid load feedback correction layer

When the proportion of EVs that temporarily change travel plan increases, the error of the V2G equivalent load

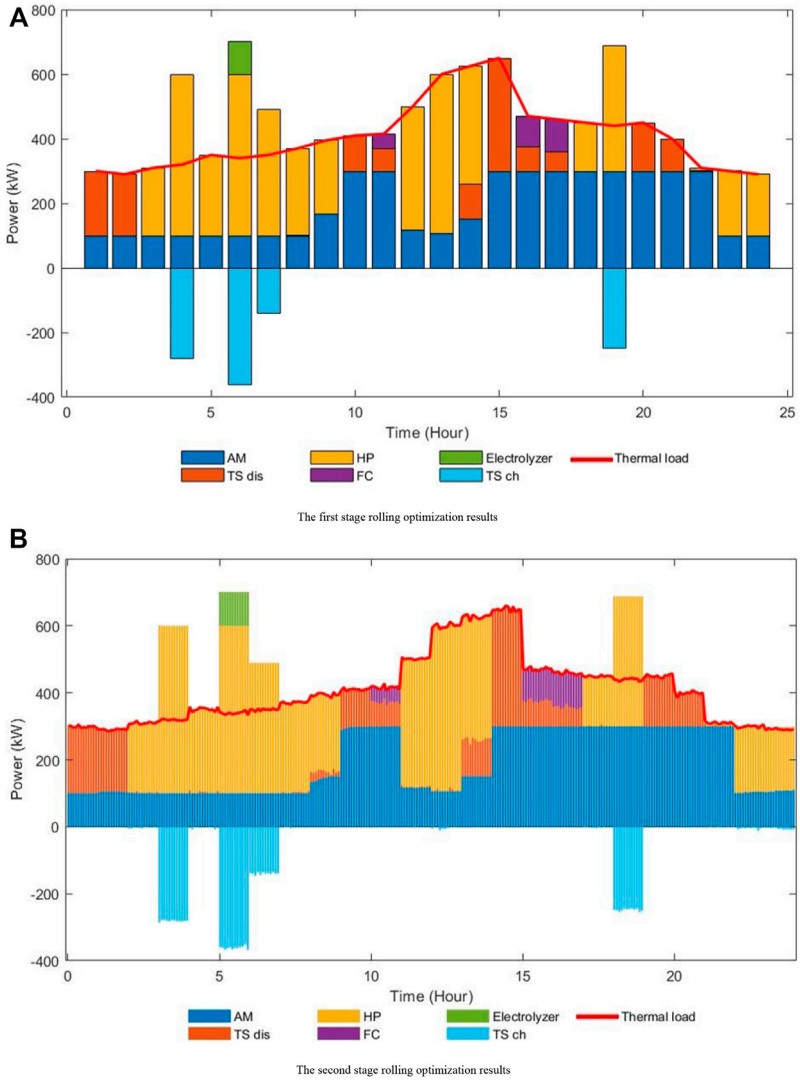

FIGURE 7
Summer thermal optimization results of MPC rolling optimization layer.

corresponding to the original plan will also increase. If the rolling optimization continues according to the original data, it will deviate from the global optimal scheduling strategy, which will make the operation economy worse, and the scheduling power deviation caused by this is not conducive to the safe and stable operation of the system. Therefore, it is necessary to re-optimize its charging and discharging power based on the actual EV travel plan. The objective of this layer is to optimize the economy of EV charging and discharging and minimize the dissatisfaction of EV owners. The specific objective function is as follows:

1) Objective function 1:

$$minF_1^{correct} = \sum_{t=1}^{T} price(t) \cdot P_{V2G}(t) \tag{45}$$

2) Objective function 2:

$$minF_2^{correct} = \frac{\sum_{n=1}^{N_{EV}} \sum_{t=1}^{T} C_B^n(t) - C_B{}^{\min}}{C_B{}^{\max} - C_B{}^{\min}} \tag{46}$$

5 Multi-objective improved sparrow search algorithm

In this paper, multi-objective improved sparrow search algorithm (MISSA) is used to solve the EV charging and

TABLE 3 Index comparison under different strategies.

Scheduling strategy	Scheduling cost(RMB)	Dissatisfaction of EV owners	Load variance(kW^2)	Comprehensive satisfaction
1	5,517.66	1	5,273	0.501
2	7,212.41	0.0876	9,149	0.412
3	6,103.24	0.2467	6,511	0.659

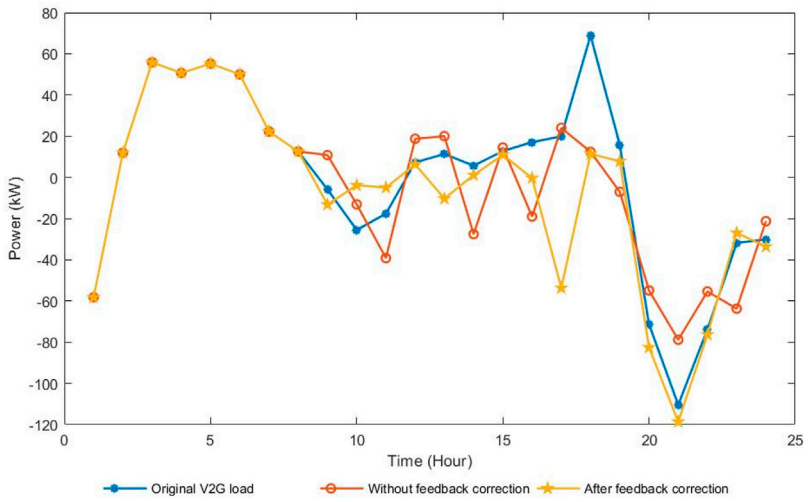

FIGURE 8
Comparison of V2G equivalent load before and after running V2G load feedback correction layer.

discharging management layer and V2G load feedback correction layer, and CPLEX is used to solve the MPC rolling optimization layer. Based on SSA (Xue and Shen, 2020), ISSA introduces Levy flight strategy to make its step size obey heavy tail distribution and improve global optimization ability (Jia et al., 2022). Furthermore, in order to make it have multi-objective optimization ability, this paper introduces elite strategy, fast non-dominated sorting strategy, congestion and congestion comparison operator.

In order to solve the mixed integer non-linear programming problem in multiple random scenes, this paper combines the Monte Carlo simulation method with the MISSA to obtain the EV charging and discharging optimization strategy. The algorithm flow chart is shown in Figure 4.

6 Simulation results and discussion

6.1 Parameter setting

It is assumed that there are 60 EVs connected to the system and all EVs are divided into four categories. Category ① EVs always have no travel plans; Category ② EVs travel on a fixed schedule; Category ③ EVs require emergency charging and Category ④ EVs temporarily change travel plans. The basic information of the above four types EVs is simulated by Monte Carlo.

According to the parameters in Table 1, different kinds of EV loads are generated through Monte Carlo simulation. Other parameters of EV are shown in Table 2. The predicted real-time electricity price, wind power and photovoltaic power are referred in (Ju et al., 2018). The pollutant treatment cost and pollutant emission coefficient of micro gas turbine are referred in (Jia et al., 2022).

MISSA parameters are set as follows: population size n = 100, maximum iterations $iter_{max}$ = 1000. In gamma function of Levy flight strategy, β = 1.5. The number of Monte Carlo simulation scenes is 500.

6.2 Result analysis

6.2.1 Scheduling results of model predictive control rolling optimization layer

As shown in Figure 5A, from 4:00 to 7:00, the electric load is low and the electricity price is relatively cheap. The excess electric

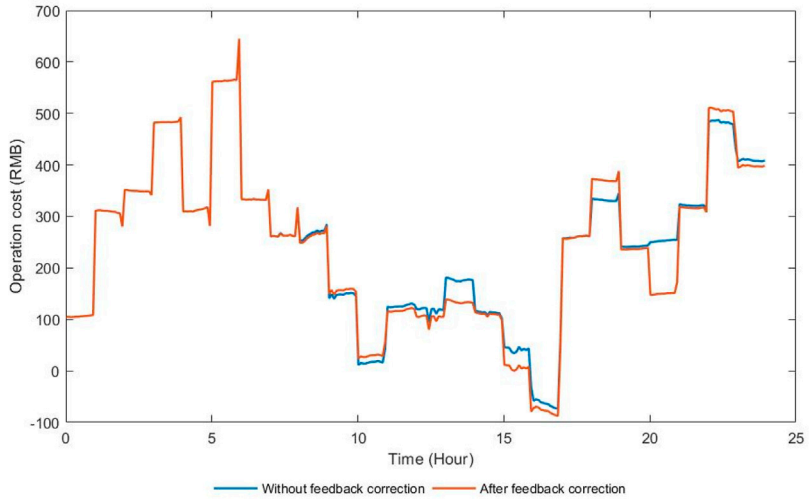

FIGURE 9
Hourly cost change of MPC rolling optimization layer.

energy is stored in the battery, converted into hydrogen energy and stored in the hydrogen storage tank. From 10:00 to 11:00 and from 15:00 to 17:00, the electricity price is high, and the electric energy will be released on the basis of meeting the power demand, so as to sell electricity to the grid as much as possible to maximize economic benefits. The coordination of electric hydrogen thermal coupling equipment ensures the economy of system operation.

As shown in Figure 5B, since the predicted power error is superimposed on the wind power photovoltaic output and load power, it is essential to coordinate each distributed generator to balance the resulting power deviation in real-time scheduling. It can be seen that supercapacitor and battery are preferred in the dispatching process. If the power deviation is still not met, the planned value of micro gas turbine and tie-line power will be changed.

As shown in Figure 6A, From 3:00 to 7:00, the electricity price is low, and the equivalent heat production cost is relatively low. The excess heat energy is stored in the heat storage device while meeting the heat load demand. From 10:00 to 17:00, the electricity price is relatively high, and the heat storage device outputs large power, reducing the output of electrothermal coupling equipment, so as to reduce the power purchase of the power grid and maintain the high economy of system operation. As shown in Figure 6B, the output of each unit in the heat network part is almost consistent with the first-stage dispatch plan value, and the predicted power error is mainly balanced by the thermal storage device.

As shown in Figures 7A,B, the thermal load characteristics in summer are quite different from those in winter. The electricity price is higher from 14:00 to 17:00. Thus, the heat storage device releases as much as possible, reducing the output of electrothermal coupling equipment, thereby reducing the power purchase. During the whole dispatching period, the thermal storage device stores heat in the low electricity price period, and releases heat in the high electricity price period, so as to reduce the system operation cost.

Compare and analyze three different strategies. Strategy 1 is to reduce the variance of load curve at all costs only from the operator's own interests; strategy 2 only considers the wishes of EV owners and charges and discharges EVs disorderly; strategy 3 comprehensively considers the interests of both sides. As shown in Table 3, compared with strategy 1, the dissatisfaction of EV owners decreased by 0.7533, the scheduling cost of the proposed strategy increased by 10.61%, and the load variance increased by 23.48%; Compared with strategy 2, the scheduling cost decreased by 15.38%, the load variance decreased by 28.83%, and the dissatisfaction of EV owners increased by 0.1591. According to the fuzzy membership function, the proposed strategy has the highest comprehensive satisfaction, which indicates that it comprehensively considers the interests of both sides, and truly achieves a win-win situation.

6.2.2 Verification of the vehicle to grid load feedback correction layer

Make 20% of category ① EVs temporarily change their plans and leave at 8:00. Compare with the circumstances without V2G load feedback correction layer. As shown in Figures 8, 9, the revised V2G equivalent load shifts the load from the period of higher electricity price to the lower period. The total operating cost with feedback correction is 5,858.2 RMB, which is 4.19% lower than that of 6,114.3 RMB without feedback correction.

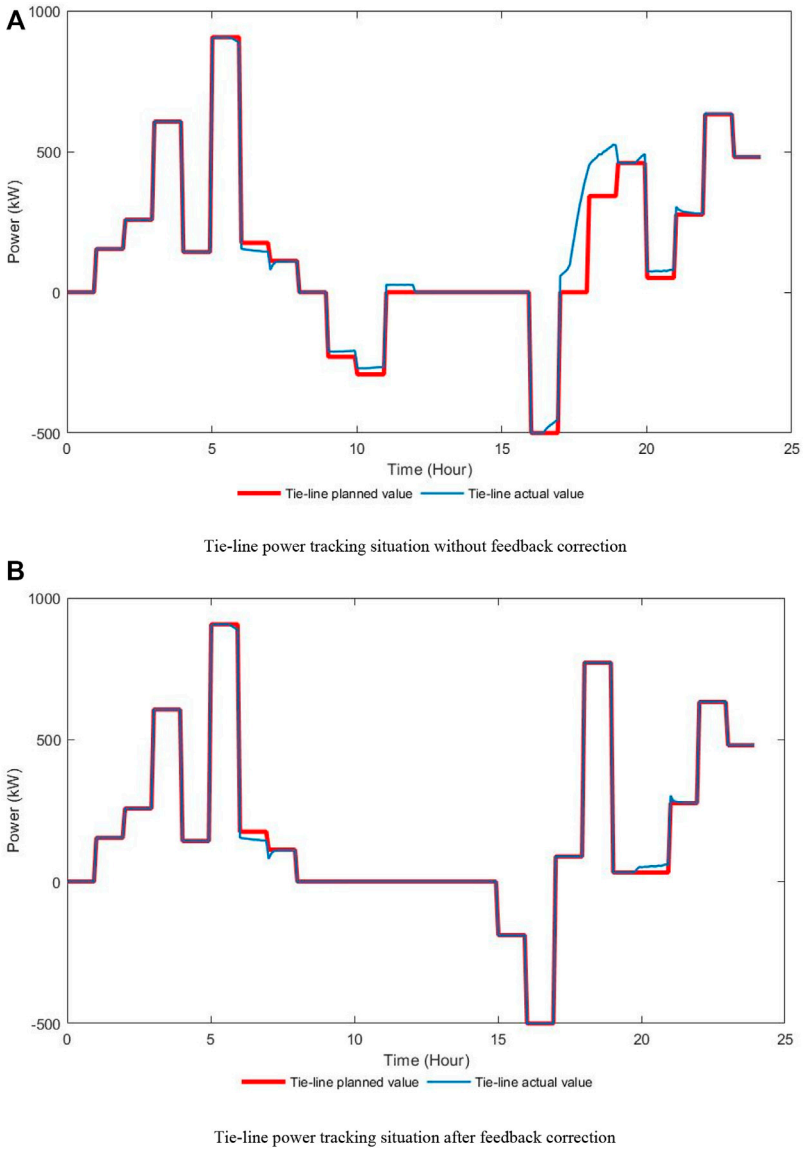

FIGURE 10
Tie-line power tracking situation. **(A)** Tie-line power tracking situation without feedback correction. **(B)** Tie-line power tracking situation after feedback correction.

In order to further verify the effect of V2G load feedback correction layer on the tracking situation of tie-line planned value, 12 EVs are charged urgently during 10:00–2:00 and 18:00–19:00. It can be seen from Figures 10A,B that the strategy with feedback correction adjusts the tie-line planned value in the scheduling process, ensuring the economic and stable operation of the system after temporarily changes of EVs' travel plan. Without feedback correction, the power relative tracking deviation of tie-line planned value is 8.82%, while the relative deviation with feedback correction is only 1.33%.

6.2.3 The effect of the unplanned Electric vehicles' proportion on scheduling results

As shown in Figure 11A, with the increase of the proportion of unplanned EVs, the deviation of original EV charging and discharging plan relative to the optimal plan in the actual situation is farther, and the economic benefit of the system operation after V2G load feedback correction is more obvious, so the relative cost change will greatly increase.

As shown in Figure 11B, the increase in the proportion of unplanned EVs will lead to the increase of source-load

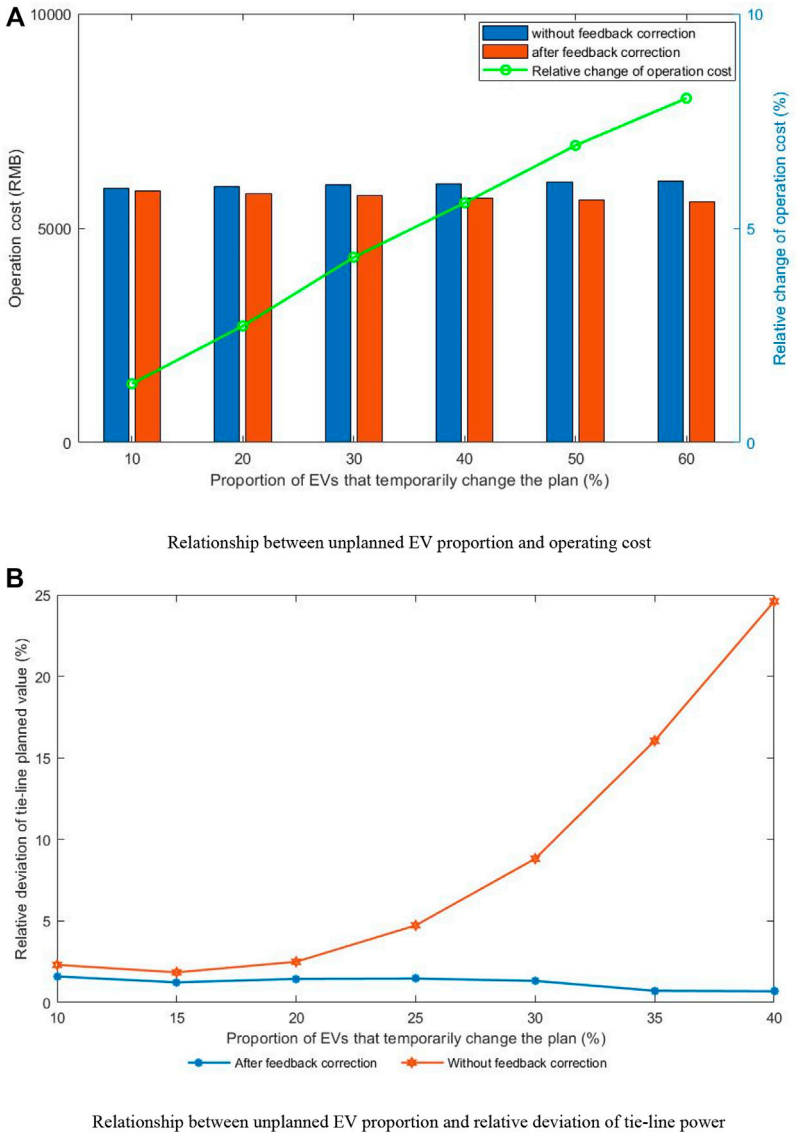

FIGURE 11
Influence of unplanned EV ratio on Scheduling Results. **(A)** Relationship between unplanned EV proportion and operating cost. **(B)** Relationship between unplanned EV proportion and relative deviation of tie-line power.

unbalanced power when operating according to the original plan. At this time, in the second stage of MPC rolling optimization layer, the output of other distributed generators is preferentially adjusted to balance the power deviation. However, when the unbalanced power is too high, the tie-line power has to be changed to maintain the source-load balance relationship. Therefore, with the increase of unplanned EVs' proportion, the relative tracking deviation of tie-line planned value without feedback correction increases greatly, while the relative tracking deviation with feedback correction is basically unchanged.

7 Conclusion

Aiming at the adverse effects of the temporary change of EVs' travel plan on the economic operation of the system and the tracking situation of tie-line planned value, this paper proposes a multi-layer coordinated optimization strategy of ETH-IES with EVs, which includes the feedback correction of V2G load. Taking an electric-thermal-hydrogen integrated energy industrial park as an example for research and analysis. The main conclusions are as follows:

1) The constructed multi-objective EV charging and discharging management model and two-stage MPC rolling optimization model can achieve accurate and win-win optimal scheduling.
2) Based on the two-layer optimization of EVs and ETH-IES, V2G load feedback correction is introduced. This can eliminate the adverse effect of EV unplanned behaviors, which improves the system economy and improves the tracking situation of tie-line planned value.
3) The coupled Monte Carlo simulation and multi-objective improved sparrow search algorithm can efficiently solve the proposed multi-objective optimal scheduling model with uncertain parameters.
4) The effectiveness of V2G load feedback correction is verified. In addition, as the proportion of unplanned EVs increases, the economic benefit is more obvious and the relative tracking deviation of tie-line planned value is basically unchanged.

Data availability statement

The raw data supporting the conclusion of this article will be made available by the authors, without undue reservation.

Author contributions

All authors listed have made a substantial, direct, and intellectual contribution to the work and approved it for publication.

Funding

This work is supported by Shaanxi Key R&D Project (No. 2019ZDLGY18-06.) and State Grid Shaanxi Electric Power Company Sci&Tech Project (No. B626KY190001). The funder was not involved in the study design, collection, analysis, interpretation of data, the writing of this article, or the decision to submit it for publication.

Conflict of interest

The authors declare that this study received funding from State Grid Shaanxi Electric Power Company. The funder was not involved in the study design, collection, analysis, interpretation of data, the writing of this article, or the decision to submit it for publication.

Publisher's note

All claims expressed in this article are solely those of the authors and do not necessarily represent those of their affiliated organizations, or those of the publisher, the editors and the reviewers. Any product that may be evaluated in this article, or claim that may be made by its manufacturer, is not guaranteed or endorsed by the publisher.

References

Alireza, A., Davoud, S., and Mostafa, S. (2021). Two-stage stochastic operation considering day-ahead and real-time scheduling of microgrids with high renewable energy sources and electric vehicles based on multi-layer energy management system. *Electr. Power Syst. Res.* 201, 107527. doi:10.1016/j.epsr.2021.107527

Chen, M., Gao, J., Chang, G., and Bai, F. (2020). Research on orderly charging strategy of micro-grid electric vehicles in V2G model. *Power Syst. Prot. Control* 48, 08.141–148. doi:10.19783/j.cnki.pspc.190697

Cheng, H., Hu, X., Wang, L., Liu, Y., and Yu, Q. (2019). Review on research of regional integrated energy system planning. *Automation Electr. Power Syst.* 43, 72–13.

Cheng, S., Wang, Y., Liao, W., Zuo, X., and Dai, J. (2022). Bi-level multi-objective optimization of a new energy microgrid with electric vehicles. *Power Syst. Prot. Control* 50, 1263–1271. doi:10.19783/j.cnki.pspc.211149

Cheng, S., Wei, Z., and Zhao, Z. (2021). Decentralized scheduling optimization for charging-storage station considering multiple spatial-temporal transfer factors of electric vehicles. *Int. J. Energy Res.* 45 (5), 6800–6815. doi:10.1002/er.6272

Colleen, S. (2008). *PEM fuel cell modeling and simulation using matlab*. Academic Press. 9780123742599. Page ix. doi:10.1016/B978-012374259-9.50001-X

Ding, T., Mu, C., Bie, Z., Du, P., Fan, Z., Zou, Z., et al. (2018). Review of energy Internet and its operation. *Proc. CSEE* 38 (15), 4318–4328.

Hou, H., Xue, M., Chen, G., Tang, J., Xu, T., and Liu, P. (2019). Multi-objective hierarchical economic dispatch for microgrid considering charging and discharging of electric vehicles. *Automation Electr. Power Syst.* 43, 1755–1762.

Hu, J., Zhou, H. R., and Li, Y. (2019). Real-time dispatching strategy for aggregated electric vehicles to smooth power fluctuation of photovoltaics. *Power Syst. Technol.* 43 (7), 2552–2560.

Hu, Z., Zhan, K., Xu, Z., Xiang, D., and Zhang, H. (2015). Analysis and outlook on the key problems of electric vehicle and power grid interaction. *Electr. Power Constr.* 36, 76–13.

Huang, W., Huang, T., Zhou, H., Wang, G., and Cui, Y. (2014). Dynamic economical dispatch for microgrid based on improved differential evolution algorithm. *Automation Electr. Power Syst.* 38 (9), 211–217.

Jia, S., Kang, X., Cui, J., Tian, B., and Xiao, S. (2022). Hierarchical stochastic optimal scheduling of electric thermal hydrogen integrated energy system considering electric vehicles. *Energies* 15, 5509. doi:10.3390/en15155509

Jia, S., and Kang, X. (2022). Multi-objective optimal scheduling of CHP microgrid considering conditional value-at-risk. *Energies* 15, 3394. doi:10.3390/en15093394

Jozi, F., Abdali, A., Mazlumi, K., and Hosseini, S. H. (2022). Reliability improvement of the Smart distribution grid incorporating EVs and BESS via optimal charging and discharging process scheduling. *Front. Energy Res.* 10, 920343. doi:10.3389/fenrg.2022.920343

Ju, C., Wang, P., Goel, L., and Xu, Y. (2018). A two-layer energy management system for microgrids with hybrid energy storage considering degradation costs. *IEEE Trans. Smart Grid* 9, 66047–66057. doi:10.1109/TSG.2017.2703126

Li, J., Wu, L., Zhang, H., Wang, W., and Jia, R. (2021). Economic dispatch of CCHP microgrid based on sorting cross optimization algorithm. *Power Syst. Prot. control* 49, 18137–18145. doi:10.19783/j.cnki.pspc.201556

Li, K., Shao, C., Wang, Y., Yan, S., Zhou, Q., Wang, X., et al. (2022). Urban integrated energy system planning considering electric-gas-traffic coupling. *J. Electr. Eng. China*, 1–10.

Li, Y., Yang, Z., Li, G., Zhao, D., and Tian, W. (2019). Optimal scheduling of an isolated microgrid with battery storage considering load and renewable generation uncertainties. *IEEE Trans. Ind. Electron.* 66 (2), 1565–1575. doi:10.1109/TIE.2018.2840498

Lv, T., Ai, Q., and Zhao, Y. (2016). A bi-level multi-objective optimal operation of grid-connected microgrids. *Electr. power Syst. Res.* 131, 60–70. doi:10.1016/j.epsr.2015.09.018

Qi, Z. Y., Li, X. W., Zhang, R. Y., Wang, Q., and Wang, J. W. (2022). Coordinated optimal scheduling of stand-alone micro-grid based on dynamic feedback correction. *High. Volt. Eng.* 48 (03), 938–947. doi:10.13336/j.1003-6520.hve.20210263

Smith, K., Earleywine, M., Wood, E., and Pesaran, A. K. (2012). Battery wear from disparate duty-cycles: Opportunities for electric-drive vehicle battery health management. *The 2012 American Control Conference*.

Tang, X., Hu, Y., Geng, Q., and Xu, X. (2021). Multi-time-scale optimal scheduling of integrated energy system considering multi-energy flexibility. *Automation Electr. Power Syst.* 45, 0481–0490.

Vetter, J., Novák, P., Wagner, M. R., Veit, C., Möller, K. C., Besenhard, J. O., et al. (2005). Ageing mechanisms in lithium-ion batteries. *J. Power Sources* 147 (1–2), 269–281. doi:10.1016/j.jpowsour.2005.01.006

Wang, J., Wang, L., Guo, Y., Sun, Y., and Guan, C. (2016). Microgrid economic dispatch method considering electric vehicles. *Power Syst. Prot. Control* 44, 17111–17117.

Wang, L., Zhou, J., Zhu, L., Wang, L., Yin, C., and Cong, H. (2021). Multi-time-scale optimization scheduling of integrated energy system based on distributed model predictive control. *Automation Electr. Power Syst.* 45, 1357–1365.

Wang, X., Guo, Q., Sun, H., Ge, H., Xin, S., Zhang, Y., et al. (2015). Distributed voltage stability assessment and control considering electric vehicle charging and discharging load. *Power Syst. Prot. Control* 43, 1643–1648.

Wang, Y., Dong, W., and Yang, Q. (2022). Multi-stage optimal energy management of multi-energy microgrid in deregulated electricity markets. *Appl. Energy* 301, 118528. doi:10.1016/j.apenergy.2022.118528

Xiao, H., Pei, W., and Kong, L. (2016). Multi-time scale coordinated optimal dispatch of microgrid based on model predictive control. *Automation Electr. Power Syst.* 40, 18.7–14+55.

Xu, Y., Zhang, R., Dong, Z., Zhang, R., and Wong, K. P. (2015). Optimal placement of static compensators for multi-objective voltage stability enhancement of power systems. *IET Gener. Transm. &amp. Distrib.* 9 (15), 2144–2151. doi:10.1049/iet-gtd.2015.0070

Xue, J., and Shen, B. (2020). A novel swarm intelligence optimization approach: Sparrow search algorithm. *Syst. Sci. Control Eng.* 8, 122–134. doi:10.1080/21642583.2019.1708830

Yang, J., Zhang, N., Wang, Y., and Kang, C. (2018). Multi-energy system towards renewable energy accommodation: Review and prospect. *Automation Electr. Power Syst.* 42 (4), 11–24.

Yin, S., Zhang, P., Yang, M., Bai, H., and Yang, Q. (2020). bMulti-time scale optimal scheduling of integrated energy system considering demand-side response. *Proc. CSU-EPSA* 32, 1135–1142. doi:10.19635/j.cnki.csu-epsa.000435

Zhang, Y., Zhang, T., Meng, F., Wang, Y., and Liu, Y. (2017). Model predictive control based distributed optimization and scheduling approach for the energy internet. *Proc. CSEE* 37, 236829–236845+7074.

Zhao, X., Wang, S., Wu, X., and Liu, J. (2016). Coordinated control strategy research of micro-grid including distributed generations and electric vehicles. *Power Syst. Technol.* 40, 123732–123740.

Zhou, J., Wu, Y., Dong, H., He, J., Xu, C., and Gao, J. (2021). Optimization planning of wind-photo-hydrogen integrated energy system considering random charging of electric vehicles. *Power Syst. autom.* 45, 2430–2440.

Nomenclature

α charge transfer coefficient

n protons exchanged per mole of reactant

F Faraday constant

P_t^{EL} power consumption of electrolyzer at time t

λ_{H_2} power consumption coefficient of hydrogen production

$H_2^{EL,t}$ hydrogen production of electrolyzer at time t

$H_2^{st,t}$ hydrogen stored at time t

$H_{2,in}^{st,t-1}$, $H_{2,out}^{st,t-1}$ hydrogen stored and released at time t-1

R_c Avogadro constant

K Kelvin temperature

$Sohc_t$ state of hydrogen charge of storage device at time t

V_{sto} volume of hydrogen storage tank

a, b proportional coefficients

$P_{sto,rated}^{H_2}$ rated pressure of hydrogen storage device

C_{re} battery replacement cost

η_{Bc}, η_{Bd} charge and discharge efficiency coefficient

E_{BA} actual full capacity of the battery

P_{load} load power value

$Mean(P_{load})$ average load power

F_1^{EV} the variance of load curve

N_{EV} total number of EVs

$C_B{}^{\min}$, $C_B{}^{\max}$ minimum and maximum affordable EV degradation costs when signing the agreement

price real-time electricity price

P_{V2G} V2G equivalent load

F_2^{EV} dissatisfaction of EV owners participating in V2G mechanism

I_n^{cha}, I_n^{dis} the n – th EV's charging and discharging signs

P_{EV}^n the n – th EV's charging and discharging power

f_{mt} fuel consumption factor

C_{mt} fuel cost factor of micro gas turbine

N total number of Monte Carlo simulation scenarios

C_{mts} start-up cost of micro gas turbine

S micro gas turbine's start-stop state

$CeSO_2$, $CeCO_2$, $CeNO_x$ unit pollution gas control cost

E_{SO_2}, E_{CO_2}, E_{NO_x} pollution gas emission

P_E electrolyzer's output power

P_t^{EL}, $P_{\min}^{EL}$, $P_{\max}^{EL}$ power of the electrolyzer and its upper and lower limits

$\Delta P_{\min}^{EL}$, $\Delta P_{\max}^{EL}$ upper and lower limits of the climbing rate of the electrolyzer

S_{ES} rated capacity of thermal storage device

P_{FC} PEMFC's output power

Q_{CS} thermal storage device's output power

$Q_{ch.\max}$, $Q_{dis.\max}$ maximum charging and discharging power of thermal storage device

Q_{load} thermal load power

ε maximum change range of battery SOC change after a scheduling cycle

U_{Buy}, U_{Sell} status of purchasing and selling

R_{up}, R_{down} MT's maximum rising rate and falling rate

U_{t-k+1} start-stop state of micro gas turbine at time t-k+1

T_{mup}, T_{mdown} minimum start time and stop time

$U_{\mathrm{Batt.ch}}$, $U_{\mathrm{Batt.dis}}$ battery charge and discharge status

$SOC_{\min}$, $SOC_{\max}$ allowable range of battery SOC in operation

$P_{ch.\max}, P_{dis.\max}$ battery's maximum charging and discharging power

$Y_{st,t}^{H_2}$ status of hydrogen storage equipment

$H_{2,in}^{st,\max}$, $H_{2,out}^{st,\max}$ maximum storage and discharge volume of hydrogen

$H_2^{st,rated}$ rated capacity of hydrogen storage equipment

$\lambda_{\min}$, $\lambda_{\max}$ minimum and maximum capacity factor of thermal storage device